C. R. Mecanique 341 (2013) 776–792

Contents lists available at ScienceDirect

Comptes Rendus Mecanique

www.sciencedirect.com

Model reduction through identification – Application to some diffusion–convection problems in heat transfer, with an extension towards control strategies

Yassine Rouizi [a,b,*], Yann Favennec [c], Yvon Jarny [c], Daniel Petit [b]

[a] *Laboratoire de mécanique et d'énergétique d'Évry, 40, rue du Pelvoux, CE1455 Courcouronnes, 91020 Évry cedex, France*
[b] *Institut P' CNRS–ENSMA–Université de Poitiers, UPR 3346, Département Fluides, Thermique, Combustion, ENSMA – Téléport 2, 1, avenue Clément-Ader, BP 40109, 86961 Futuroscope-Chasseneuil-du-Poitou cedex, France*
[c] *Laboratoire de thermocinétique de Nantes, UMR–CNRS 6607, École polytechnique de l'université de Nantes, La Chantrerie, 44306 Nantes cedex 3, France*

ARTICLE INFO

Article history:
Received 5 April 2013
Accepted after revision 27 September 2013
Available online 12 November 2013

Keywords:
Feedback control
Model reduction
Modal identification method
Optimization
Backward-facing step flow
Heat transfer convection

ABSTRACT

The simulation of heat convection problems usually leads to very large matrix systems because both Navier–Stokes equations and the energy equations are to be taken into account and discretized. Of course, such large matrix systems cannot be used for on-line control algorithms due to memory limitations and computation time. On-line control algorithms should rather consider much smaller matrix systems. Bearing this in mind, model reduction techniques present a large interest to obtain a suitable low-order model that can further be used in control processes. In this paper, reduced models are obtained through the modal identification method. This method relies on the solution of an optimization problem of parameter estimation following the steps: (i) the structure of the state model is first defined, (ii) the related vectors and matrices are estimated through the minimization of a corresponding functional, (iii) the reduced order model then must be validated with input data different from those used within the identification process. These steps being completed, other control algorithms can "plug" such reduced models. Among linear control algorithms, the feedback control laws considered in this paper are based either on the reduced state or on the output. A Kalman filter evaluates the state through a limited number of measurements. The developed numerical application deals with a temperature field within a 2D stationary flow over a backward-facing step. The goal is to keep the outlet temperature as close as possible to a given temperature profile downstream from the step, whatever the pipe inlet temperature fluctuations. One thus searches some "optimal" heat fluxes upstream from the step that counteract the inlet temperature variations.

1. Introduction

Nowadays, the need to optimize system performance has become essential to reduce, for example, functions of production costs or production rates of pollution such as emissions of greenhouse gases. Industries being more and more confronted with this type of problem, the process control is becoming increasingly necessary. The optimal control of a system allows us to reach a satisfying final goal while respecting reverts constraints.

* Corresponding author.
E-mail address: y.rouizi@iut.univ-evry.fr (Y. Rouizi).

1631-0721/$ – see front matter
http://dx.doi.org/10.1016/j.crme.2013.09.005

In the area of heat transfer and fluid mechanics, modeling returns often to a discretization of the local equations (the energy equation and/or the Navier–Stokes equations) and then to the solution of a system of ordinary differential equations which result from the spatial discretization. This discretization, which has to correspond to a very fine meshing in order to capture the detailed physical phenomena, requires a large number of degrees of freedom for the corresponding models. In spite of the continuous increase in the computational performances of computers, detailed simulations still necessitate large computing times with large memory allocation. This makes impossible the use of such models for applications in inverse or optimal control problems. In these cases, the need to obtain reliable and fast answers is paramount. It is in this view that the methods of model reduction play a full role.

The goal of model reduction is thus to build a model of small size, allowing very short execution times with small memory allocation. Model reduction techniques are particularly adapted to real-time applications. However, the obtained Reduced Order Models (ROM) should preserve the properties of the studied physical phenomena and must also capture the essential characteristics of the model of reference to an acceptable precision.

There is an extensive bibliography in which one can find many model reduction techniques either for linear systems or for nonlinear ones. The reader interested by the techniques and the comments of these methods can refer to the more detailed reviews and articles [1–3] (to cite a few). We focus here on the use of the Modal Identification Method (MIM) to build ROM.

The MIM uses concepts stemming from the automatics community. This method has been specifically developed by the heat transfer community to identify ROM in linear thermal diffusion processes from experimental data [4]. Next, the MIM has been extended to nonlinear heat transfer [5,6]. An extension of the method to fluid flows has been proposed [7,8], the identification method being reformulated using the adjoint-state method to compute the gradient of the cost function to be minimized [9].

The Modal Identification Method relies on two main steps:

- the first stage is to define a structure of equations for the ROM. Starting from the local partial differential equations describing the physics, a state-space representation which arises from space discretization is considered as a general detailed model structure. Eventually, the ROM equations are similar to those of the state-space representation but under the modal form;
- once the structure is chosen, the next step is to identify the parameters that define the ROM through the minimization of a cost function that measures the difference between the outputs of the ROM and the outputs of the system (detailed model or real process). The identification process therefore relies on the solution of an inverse problem of parameter estimation in which the set of data to be recovered comes either from simulations performed with the detailed model or from in-situ measurements.

2. Optimal control

The PID controllers (proportional–integral–derivative) are by far the most used in industry. However, a fine adjustment of the control parameters (PID tuning) can be highly complicated especially for the Multi-Input Multi-Output systems. Indeed, when the control parameters are chosen incorrectly, the controlled process can become unstable. The objectives of the adjustment of the controller are thus, its robustness, its stability and the resulting accuracy.

The modern theory of control is based on the state-space representation. This representation makes it possible to model a dynamic system in matrix form by relating the inputs to the outputs. To do so, let us consider the following linear time-invariant state-space model:

$$\begin{cases} \dot{X}(t) = AX(t) + Bu(t) \\ Y(t) = CX(t) \end{cases} \tag{1}$$

where $X \in \mathbb{R}^n$, $u \in \mathbb{R}^p$, and $Y \in \mathbb{R}^q$ are the state, the control input, and the controlled output, respectively, and A, B and C are the corresponding matrices. The optimal feedback control process consists in acting on the control input $u(t)$ so that the outputs of the system stored in Y present the wished characteristics. The use of optimal feedback controllers is particularly suited when the dynamics of the system is known in spite of the disturbances, as well as for Multi-Inputs/Multi-Outputs (MIMO) systems. Optimal control deals with the problem of finding a control law for a given system in such manner that a certain optimality criterion is satisfied. Besides, this paper rather focuses on the feedback controllers based on quadratic cost functions, i.e. on LQ controllers (LQ standing for Linear Quadratic). In the present work, two optimal feedback control problems are considered: the tracking problem and the regulator problem, the state-space model being given through the use of model identification techniques.

2.1. Tracking problem

Let us first consider the tracking problem where the aim is to find the optimal command that makes the system follow a prescribed trajectory. This is performed by minimizing the following cost function:

$$\mathcal{J} = \int_{\mathcal{I}} \left[\varepsilon^T Q\,\varepsilon + u^T \ell_p^2 u\right] \mathrm{d}t \tag{2}$$

where $\varepsilon = Y - Y_c$ is the tracking error that integrates the difference between the output model Y and the desired output Y_c, $\mathcal{I}$ denotes a time range, Q is a weighting matrix and ℓ_p^2 is the diagonal matrix $\ell^2 I_p$ (with I_p the identity matrix of dimension p), and ℓ is a parameter that penalizes excessive control input magnitudes. When considering the tracking problem, the error depends on time, thus $\varepsilon = \varepsilon(t)$, and inputs are also time-dependent, thus $u = u(t)$.

In order to obtain the optimal command (i.e. the minimum of the cost function $\mathcal{J}$), the Hamiltonian function

$$\mathcal{H} = \varepsilon^T Q\,\varepsilon + u^T \ell_p^2 u + \lambda^T (AX + Bu) \tag{3}$$

is introduced with λ the co-state variable. The differentiation of $\mathcal{H}$ with respect to X, u and λ leads to the equations of optimality [10]:

$$-\dot{\lambda} = \frac{\partial \mathcal{H}}{\partial X} = A^T \lambda + C^T Q\,C X - C^T Q\,Y_c \tag{4}$$

$$0 = \frac{\partial \mathcal{H}}{\partial u} = \ell_p^2 u + B^T \lambda \tag{5}$$

$$\dot{X} = \frac{\partial \mathcal{H}}{\partial \lambda} = AX + Bu \tag{6}$$

In order to perform the optimal feedback control, a feedback relationship between the state X and its related co-state λ is defined:

$$\lambda = PX + L \tag{7}$$

Inserting this relationship into the adjoint equation (4) and integrating the optimality condition (5), one obtains the expression of the optimal control law:

$$u = -\left(\ell_p^2\right)^{-1} B^T P X - \left(\ell_p^2\right)^{-1} B^T L \tag{8}$$

where P and L are the so-called Riccati matrices, solutions of the differential Riccati equations:

$$\begin{aligned} &\dot{P} + PA + A^T P - PB\left(\ell_p^2\right)^{-1} B^T P + C^T Q\,C = 0 \\ &\dot{L} + A^T L - PB\left(\ell_p^2\right)^{-1} B^T L - C^T Q\,Y_c = 0 \end{aligned} \tag{9}$$

2.2. Regulation problem

Now, let us consider the regulation problem. As in [11,12], the regulation problem consists in finding the control law that minimizes the deviation δX between the actual state X and the steady optimal state $\bar{X}$ (relative to the target Y_c). This can be mathematically rephrased as minimizing:

$$\mathcal{J} = \frac{1}{2} \int_{\mathcal{I}} \left[\delta X^T Q\,\delta X + \delta u^T \ell_p^2 \delta u\right] \mathrm{d}t \tag{10}$$

where $\delta u = u - \bar{u}$ is the deviation from the optimal input. In short, the regulation problem consists in minimizing the cost function that integrates deviations from the optimal trajectory. The control u that minimizes (10) is given by [12]:

$$\delta u(t) = -\left(\ell_p^2 + B^T \Pi B\right)^{-1} B^T \Pi A \delta x(t) \tag{11}$$

where Π is the solution of the differential Riccati equation:

$$\Pi = A^T \Pi A - A^T \Pi B\left(\ell_p^2 + B^T \Pi B\right)^{-1} B^T \Pi A + C^T C \tag{12}$$

2.3. State estimation

The optimal control laws defined by (8) and (11) require the knowledge (or at least an evaluation) of the state at each discrete time. In practice, we do not have a complete knowledge of the state of the system. In this case it is necessary to introduce estimators for the state that give state approximations assimilating measurements. In the present case, the Kalman filter is used to provide an optimal estimation of the state from stochastic state propagation and from noisy observations. Let us consider the following stochastic state model:

$$\begin{cases} \dot{X}(t) = AX(t) + Bu(t) + Gw(t) \\ Y(t) = CX(t) + v(t) \end{cases} \tag{13}$$

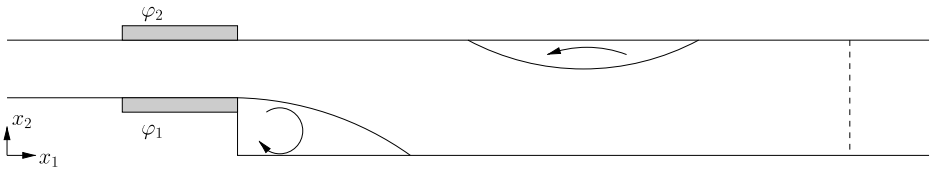

Fig. 1. The backward-facing step scheme. The upstream tube is 4*h* long; the downstream tube is 30*h* long. The dashed line represents the place where the sensors are and where the optimization is performed on.

where w is the state noise and v is the observation noise. Both noises are assumed to be white zero mean Gaussian noises and to be independent:

$$E\big[w(t)w(t+\tau)\big] = W\delta(\tau) \tag{14}$$

$$E\big[v(t)v(t+\tau)\big] = V\delta(\tau) \tag{15}$$

$$E\big[w(t)v(t+\tau)\big] = 0 \tag{16}$$

where $E[\cdot]$ is the expected value, and $\delta(\ell) = 1$ only if the integer $\ell = 0$, and $\delta(\ell) = 0$ otherwise, and matrices W and V are the covariance matrices associated with noises w and v. The Kalman filter enables on-line state estimation under assumptions presented above. The filtering problem eventually consists in evaluating the state estimation $\hat{X}$ of the real state X taking into account of outputs Y available until this moment.

To do so, let us consider the estimation error $e_x(t)$ defined by:

$$e_x(t) = X(t) - \hat{X}(t) \tag{17}$$

The Kalman filter allows us to establish the structure of the linear system providing $\hat{X}$ such as the average of the estimation error $e_x(t)$ tends towards 0 when t tends towards infinity. It gathers two differential equations, one for the state estimate and one for the covariance matrix [10]:

$$\dot{\hat{X}}(t) = \big[A\hat{X}(t) + Bu(t)\big] + K_f\big[Y(t) - C\hat{X}(t)\big] \tag{18}$$

where $K_f(t) = \Sigma C^T V^{-1}$ is the Kalman gain matrix and Σ is solution of the differential Riccati equation:

$$\dot{\Sigma} = \Sigma A^T + A\Sigma - \Sigma C^T V^{-1} C\Sigma + GWG^T \tag{19}$$

The control laws given by (8) and (11) are actually applied on state estimations $\hat{X}$ given by the integration of (18) rather than on the unknown state X. Both above presented controllers coupled with the Kalman state estimation filter are to be based on small size linear models like the ones presented in Section 4.

3. The studied system

This section describes the studied system, along with some numerical results of simulations. Let us consider a 2D incompressible laminar flow over a backward-facing step with an expansion ratio of 2.0, as schematically depicted in Fig. 1. In the present case, the upstream height and step height are $h = 1$ cm, hence the downstream height is $2h$.

The coordinate system is defined as shown schematically in this figure, where the $\vec{x}_1$ and $\vec{x}_2$ coordinate directions denote respectively the streamwise and the transverse directions. The chosen fluid which is assumed to be Newtonian and incompressible is air, with the following constant properties: dynamic viscosity $\mu = 1.81 \times 10^{-5}$ kg/(m s), density $\rho = 1.205$ kg/m^3, heat capacity $C_p = 1005$ J/(kg K), and thermal conductivity $\lambda = 0.0262$ W/(m K). A fully developed velocity profile $\boldsymbol{v}$ and a temperature T_∞ are imposed at the entrance of the channel. The flow geometry was considered by Armaly et al. [13] who chose to define the Reynolds number Re, as follows:

$$\mathrm{Re} = \frac{U_\infty 2h}{\nu} \tag{20}$$

where U_∞ is the inlet mean velocity and $\nu = \frac{\mu}{\rho}$ is the kinematic viscosity of the fluid. The use of $2h$ as the characteristic length scale is attributed to the fact that the Reynolds number is based upon the hydraulic diameter of the inlet channel. The equation that describes the parabola velocity profile at the entrance ($x_1 = -4h$ and $x_2 \in [h : 2h]$) is given by:

$$\begin{cases} \bar{u}_1(-4h, x_2) = 3\dfrac{\mathrm{Re}\nu}{h^3}(x_2 - h)(2h - x_2) \\ \bar{u}_2(-4h, x_2) = 0 \end{cases} \tag{21}$$

where (u_1, u_2) are the components of the velocity vector $\boldsymbol{v}$ in the $(\vec{x}_1, \vec{x}_2)$ coordinate directions. At the opposite, the free outflow boundary condition is considered at the outlet section. This condition assumes that the flow is fully developed at

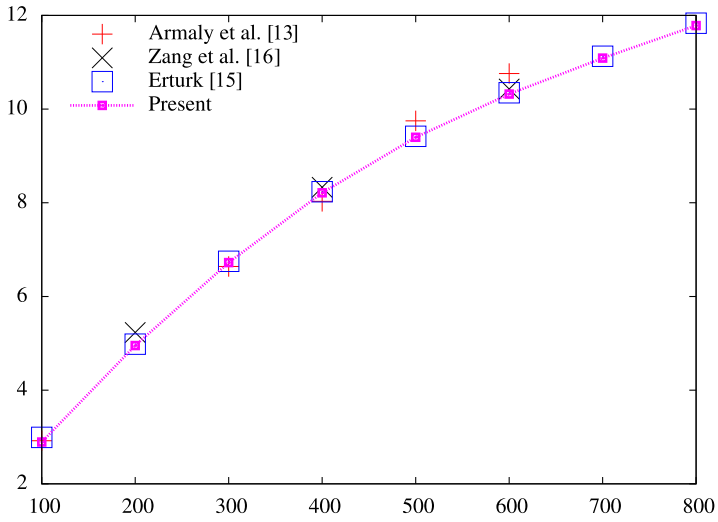

Fig. 2. Size of the main recirculation region length X_1/h as a function of the Reynolds number Re.

the outlet section. This can be done when the outlet is located far enough downstream, assuming that $\frac{\partial u_1}{\partial x_1} = 0$. On all other boundaries a null velocity is prescribed. In the present study, the flow is driven at a fixed Reynolds number equaling 500, and the velocity is assumed to be known and steady. Hence, only the energy problem is considered. At the entrance of the channel, the fluid is at temperature T_∞ and the outflow boundary condition leads to $\frac{\partial T}{\partial x_1} = 0$. Next, two uniform heaters (in terms of fluxes) are imposed on a portion of external faces. Heaters respectively located at $x_1 \in [2h : 4h]$ bottom and top (see Fig. 1) heat the flow at reason of flux density equaling respectively φ_1 and φ_2. All other boundaries but the inflow and outflow are considered as insulated. The initial condition for temperature T $(t = 0)$ is assumed to be known and equal to 300 K.

3.1. The reference model

A reference model is considered at the building-data stage before the identification of low-order models. The numerical simulations are performed with the computational fluid dynamics (CFD) software (Fluent® version 6.3.26) [14]. Grid independence tests have been performed using several grid densities, and the reattachment location on the stepped wall has been used as the mesh convergence criterion. In the present study, 144,247 nodes have been used for the computations, while respecting grid independency.

The validation of this reference model is performed for several Reynolds numbers Re within the range [100 : 800]. The numerical model is compared to the existing material from literature (experimental study provided by Armaly et al. [13] and numerical studies provided by Erturk [15] and Zang et al. [16]) through the evolution of the recirculation region length:

- for all Reynolds numbers used, there is a main recirculation region whose length X_1 increases with the Reynolds number;
- for Reynolds numbers greater than 400, a second recirculation bubble appears attached to the upper wall of the channel, between X_2 and X_3.

Figs. 2 and 3 present the evolution of lengths X_1/h, X_2/h and X_3/h with respect to the Reynolds number from 100 up to 800. It is seen that detachment and reattachment locations found by our simulations are in coherence with the results from literature. With such results, one can consider that the used numerical model is validated and is thus able to give accurate results for any Reynolds number within the considered range.

Once the fluid simulation methodology is validated, the thermal simulation in forced convection problems with the CFD code should be accurate enough, the energy equation being linear and much simpler to solve than the Navier–Stokes equations. Moreover, it can be observed that several benchmark solutions are available in the literature when the heat flux is applied in the stepped wall; however, to our knowledge, there is no benchmark solution available when the heat flux is applied in the stepped wall just before the sudden expansion region. Note again that the aim of the present paper is to give an example illustrating the use of optimal control algorithms coupled with low-order models, rather than giving a complete study of the test problem.

The objective of the present study is, in fine, to control the temperature profile on a vertical line located at $x_1 = 16h$ through the two heaters when the inlet temperature (at $x_1 = 0$) varies in time. More precisely we would like the temperature on the considered line to be as close as possible to the temperature $\tilde{T}$ whatever the inlet temperature $T_\infty(t) \leqslant \tilde{T}$.

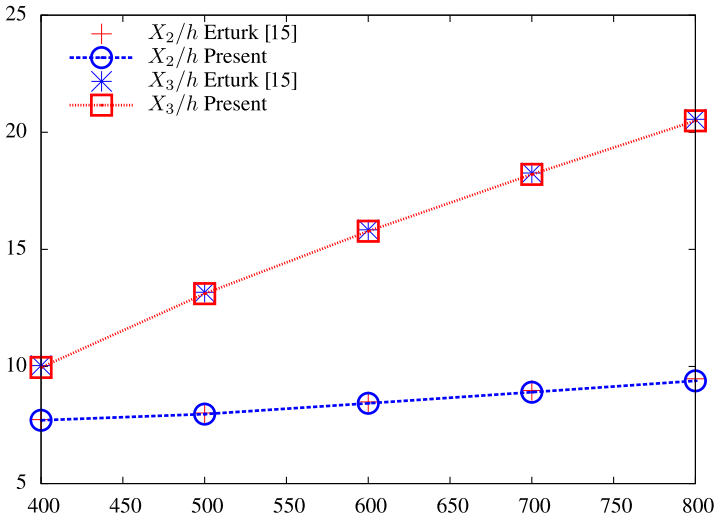

Fig. 3. The locations of the detachment point X_2/h and the reattachment point X_3/h as a function of the Reynolds number Re.

3.2. The governing equation

The energy problem for a given velocity distribution $\boldsymbol{v}$ is described by the following convection–diffusion equation:

$$\rho C_p\left(\frac{\partial T}{\partial t} + \boldsymbol{v}\cdot\nabla T\right) - \nabla\cdot(\lambda\nabla T) = 0 \tag{22}$$

where $T = T(\boldsymbol{x}, t)$ is the temperature distribution for $t \geqslant 0$ and $\boldsymbol{x} \in \Omega$. Within the scope of this paper, Ω represents the backward-facing step pipe presented schematically in Fig. 1. The boundary conditions are set as follows:

- the time-dependent inlet temperature is assumed to be x_2-independent, hence $T(\boldsymbol{x}, t) = T_\infty(t)$ for $\boldsymbol{x} \in \partial\Omega_{\text{in}}$;
- the heaters on boundaries $\partial\Omega_{\varphi_k}$ deliver a known prescribed flux density φ_k, hence $\lambda\nabla T\cdot\boldsymbol{n} = -\varphi_k$ for $\boldsymbol{x} \in \partial\Omega_{\varphi_k}$, $k = 1, 2$ with $\boldsymbol{n}$ the outward unit normal vector;
- the zero diffusion flux condition is applied at the outflow boundary as the flow is assumed to be thermally fully developed;
- the null flux is applied on all other boundaries, then $\nabla T\cdot\boldsymbol{n} = 0$ for $x \in \partial\Omega_{\text{wall}}\backslash(\partial\Omega_{\varphi_k}\cup\partial\Omega_{\text{in}})$;
- the initial condition $T(\boldsymbol{x}, 0) = T_0(\boldsymbol{x})$ is also considered at time $t = 0$.

The space discretization of the partial differential equation (22) with above-considered boundary conditions leads to the set of ordinary differential equations presented in matrix form as:

$$\dot{T} = \mathcal{A}T + \mathcal{B}u + \mathcal{G}T_\infty \tag{23}$$

where $\mathcal{A}$ gathers both the convection operator $(\boldsymbol{v}\cdot\nabla)$ and the diffusion operator $(\nabla\cdot\lambda\nabla)$, $\mathcal{B}$ is the command matrix relative to the flux input vector $u(t) = [\varphi_1(t), \varphi_2(t)]^T$ and $\mathcal{G}$ is the operator that applies the inlet Dirichlet boundary condition to the system. Note that the temperature variables T in (23) and T in (22) have a very different meaning since T in (22) represents the space-continuous temperature variable while T in (23) represents the semi-discretized temperature variable. The solution of (23) gives the temperature response $T(t)$ for a given inlet temperature $T_\infty(t)$ and input flux $u(t)$ and with a given initial condition $T(0) = T_0$. The number N of differential equations involved in (23) depends on the discretization type and fineness. This set of ordinary differential equations (23) is coupled with an output equation for space selection:

$$Y = \mathcal{C}T \tag{24}$$

where $Y \in \mathbb{R}^q$, $q \leqslant N$ and $\mathcal{C}$ is the observation matrix which allows to select a part of the whole temperature field. The output Y actually represents the quantity of interest for control applications detailed later on. Note that whatever the discretization type and fineness, the number N of differential equations involved in (23) is likely to be by far too large for most real on-line control applications. A way to reduce the number of differential equations in (23) (or in any other equivalent system) is to consider model reduction approaches.

4. Model reduction

The numerical solution of fluid mechanics and thermal problems usually needs a fine spatial discretization of the considered domain. Consequently, the matrix systems may be large and the computational times may be elevated. Although these

models may be highly reliable and accurate, the computational cost can be too high to treat applications such as real-time control and inverse problems for instance. The alternative is to build a reduced order model (ROM) that contains a much lower number of degrees of freedom and that still reproduces well enough the dynamics of the reference model.

Many reduction methods have been developed, for linear or nonlinear problems. Within the field of fluid mechanics, the most commonly-used approach is the Proper Orthogonal Decomposition method coupled with a Galerkin projection of the partial differential equations (POD-G). The reader interested in reviews on such reduction techniques and others can refer to [1] or [2,3] for instance.

The technique used in this study is the Modal Identification Method (MIM). The MIM consists in identifying the components of a matrix system equivalent to (23) but written in its modal base. Only a small number of modes are considered for the identification. Usually, the MIM is coupled with iterative methods using gradient-type methods and the adjoint-state method for the computation of the objective function gradient. We describe hereafter the main features related to the MIM. The reader could refer to [17,8,18,6,9,5] for more details on recently developed numerical methods as well as related applications.

4.1. ROM structure

The first step considered within the Modal Identification Method is to define the general structure of the ROM starting from the modal structure of the Detailed Model equations (23). Let $\hat{\mathcal{A}}$ be the diagonal matrix of $\mathcal{A}$ involved in (23) and Σ the matrix of eigenvectors of $\mathcal{A}$ such that $\hat{\mathcal{A}} = \Sigma^{-1}\mathcal{A}\Sigma$, and let us perform the change of variable $T = \Sigma X$, $X \in \mathbb{R}^N$ where N is the number of degrees of freedom involved in (23). Doing so, (23) becomes:

$$\dot{X} = \hat{\mathcal{A}}X + \hat{\mathcal{B}}u + \hat{\mathcal{G}}T_\infty \tag{25}$$

where $\hat{\mathcal{B}} = \Sigma^{-1}\mathcal{B}$ and $\hat{\mathcal{G}} = \Sigma^{-1}\mathcal{G}$. The output relationship is also expressed as:

$$Y = \hat{\mathcal{C}}X \tag{26}$$

where one used $\hat{\mathcal{C}} = \mathcal{C}\Sigma$. At this stage, the modal formulation (25)–(26) is still of order N. In classical modal reduction methods, a spectral problem associated with the state matrix ($\mathcal{A}$) of Eq. (23) is solved, then the reduced models are obtained by selecting the most dominant modes ($n \ll N$ modes) according to some temporal or energetic criteria. Instead of computing these modes and selecting them afterwards, the MIM consists in identifying the components of a matrix system of the form (25)–(26) but of smaller dimension, say with the reduced order variable $x \in \mathbb{R}^n$, and output $y \in \mathbb{R}^q$:

$$\dot{x} = ax + bu + gT_\infty \tag{27}$$

$$y = cx \tag{28}$$

4.2. Principle of identification

The above developments enabled to define the form of the ROM. The approach of identification does not solve any eigenvalue problem as it is the case with most other reduction approaches. The identification procedure consists in identifying the following matrix components: n non-zero components for the diagonal matrix a, $n \times p$ components for the input matrix b, n components for the vector g, and $q \times n$ components for the selection matrix c.

The procedure of identification relies on the minimization of the mean squared discrepancy $\mathcal{J}(\theta)$. This function is based on the difference between the response of the reference model $y_j(\theta, t_k)$ and the outputs $Y_j^*(t_k)$ given by the ROM when the same input signal is applied for both (the ROM outputs implicitly depend on the parameter vector $\theta = \{a_{ii}, b_{ij}, g_i, c_{ki}\}$, $i = 1, \ldots, n$, $j = 1, \ldots, p$, $k = 1, \ldots, q$ that gathers all unknown components of (27)–(28)). More specifically, the cost function $\mathcal{J}(\theta)$ integrates the squared differences for the temperature at K time steps and at the q selected locations.

$$\mathcal{J}(\theta) = \frac{1}{2}\sum_{k=1}^{K}\sum_{j=1}^{q}\left(y_j(\theta, t_k) - Y_j^*(t_k)\right)^2 \tag{29}$$

The identification process relies on the solution of the optimization problem that consists in finding the optimal parameter vector $\bar{\theta}$ such that:

$$\bar{\theta} = \arg\min\left[\mathcal{J}(\theta)\right] \tag{30}$$

In the following applications, the BFGS quasi-Newton optimizer [19] has been used due to its inherent convergence ability and robustness.

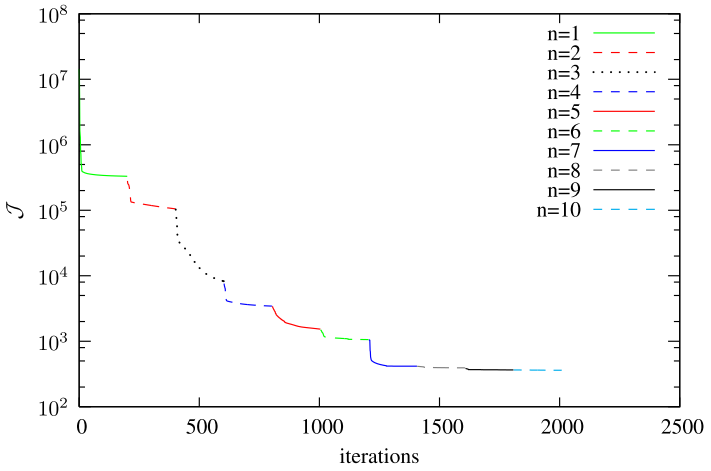

Fig. 4. Evolution of the cost function value $\mathcal{J}$ with respect to the optimization iterations for reduced model orders increasing until $n = 10$.

Table 1
Evolution of the cost function value $\mathcal{J}$ and of the mean quadratic errors σ with respect to the reduced model order n.

Order n	$\mathcal{J}$ (K^2)	σ (K)
1	0.214×10^6	0.141×10^1
2	0.221×10^5	0.452×10^0
3	0.783×10^4	0.269×10^0
4	0.234×10^4	0.147×10^0
5	0.872×10^3	0.899×10^{-1}
6	0.517×10^3	0.692×10^{-1}
7	0.334×10^3	0.556×10^{-1}
8	0.296×10^3	0.523×10^{-1}
9	0.128×10^3	0.344×10^{-1}
10	0.666×10^2	0.248×10^{-1}

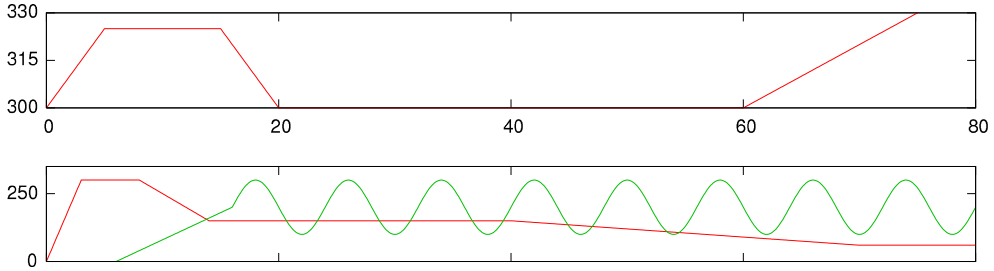

Fig. 5. Top: inlet temperature evolution (K); bottom: input flux evolution (W/m^2 – red line: φ_1, green line: φ_2). (For interpretation of the references to color in this figure legend, the reader is referred to the web version of this article.)

4.3. The reduced order model on the studied system

In order to make sure that the ROM is able to reproduce the dynamics of the three inputs together, the three inputs of the model (φ_1 and φ_2 and T_∞) have been first applied separately.

The obtained time varying temperatures, from which is subtracted the initial temperature, are then used as data for the model identification.

The initial temperature $T(x, 0)$ is taken constant at 300 K with inlet temperature also equal to 300 K and null fluxes φ_1 and φ_2. At time zero the flux φ_1 jumps from 0 to 300 W/m^2 then stays constant. At time $t = 40$ s the flux φ_2 jumps from 0 to 300 W/m^2 then stays constant. Then, at time $t = 80$ s, the inlet temperature jumps to 325 K then stays constant. This procedure is presented below:

$$\begin{cases} \varphi_1(t) = 300 \times \mathcal{H}(t) \\ \varphi_2(t) = 300 \times \mathcal{H}(t - 40) \\ T_\infty(t) = T(x, 0) + 25 \times \mathcal{H}(t - 80) \end{cases} \tag{31}$$

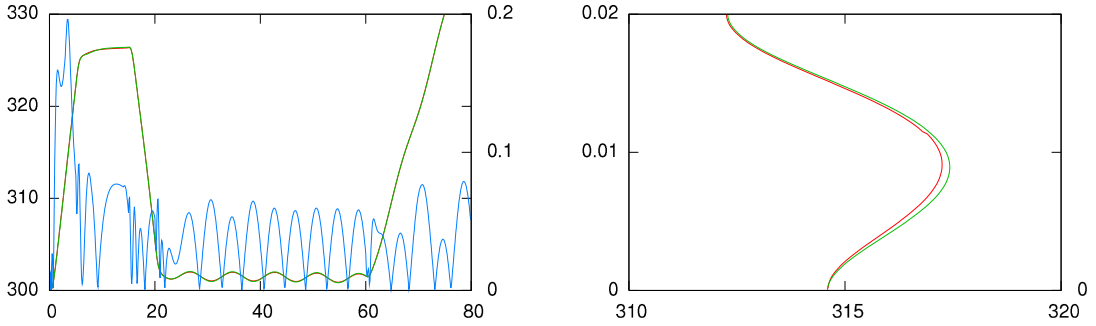

Fig. 6. Left: temperature evolution (K) for both the detailed model (green line, l.h.s.) and the six-order reduced model (red line, l.h.s.) for location $x_1 = 16h$ and $x_2 = 0$, and the absolute difference (K) between both models (blue line, r.h.s.); right: temperature profile (K) at $t = 4$ s and $x_1 = 16h$ for both the detailed model (green line) and the six-order reduced model (red line). (For interpretation of the references to color in this figure legend, the reader is referred to the web version of this article.)

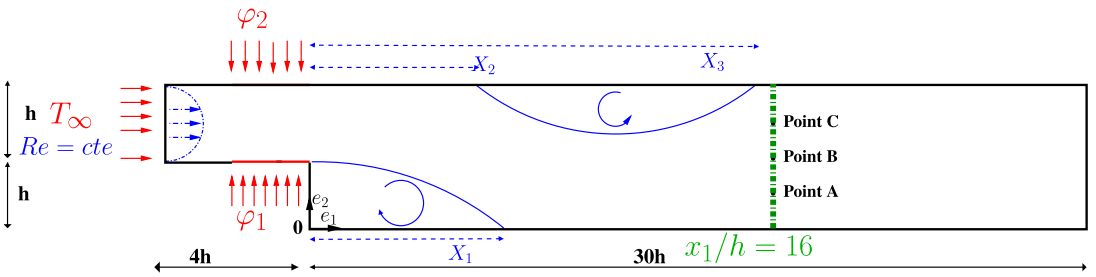

Fig. 7. Studied system.

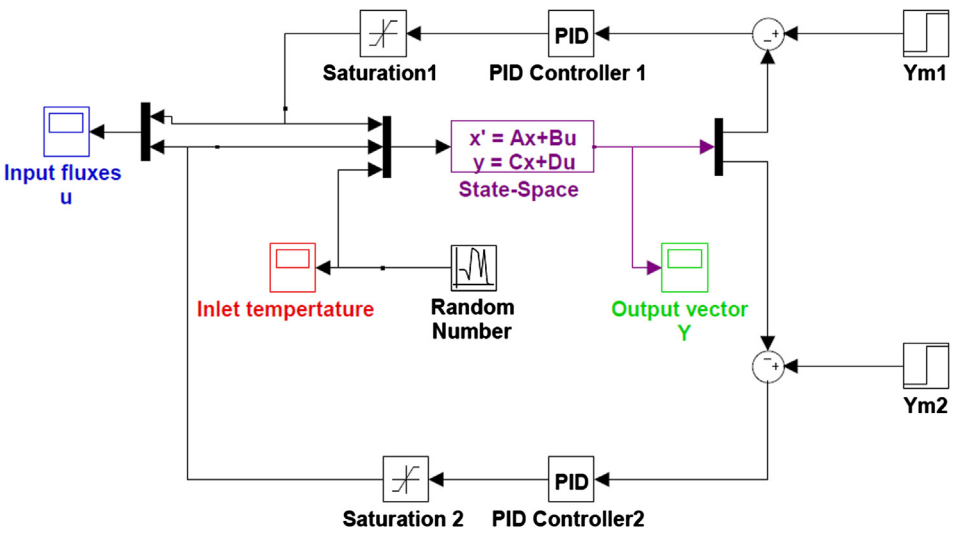

Fig. 8. Block diagram of the PID controller.

where $\mathcal{H}$ is the Heaviside step function.

Fig. 4 presents the evolution of the cost function value $\mathcal{J}$ (defined by (29)) as a function of the increasing reduced model order n and, for each order in the minimization procedure. This figure shows that for a given order the cost function $\mathcal{J}$ is still decreasing and that the cost function value is generally decreasing with respect to the reduced model order at the end of the optimization iterations. Note that roughly 200 iterations are needed for convergence for each given reduced model order. 2009 iterations in total were necessary for global convergence until order $n = 10$. Table 1 gives the evolution of the cost function and of the mean quadratic error σ (such that $\sigma^2 = 2(K \times q)^{-1}\mathcal{J}$) with respect to the reduced model order after reached inner-loop convergence.

Once the ROM has been identified, the next step is to validate it. The purpose of validation is actually to verify that the reduced model is able to reproduce the behavior of the reference model when other input evolutions are prescribed.

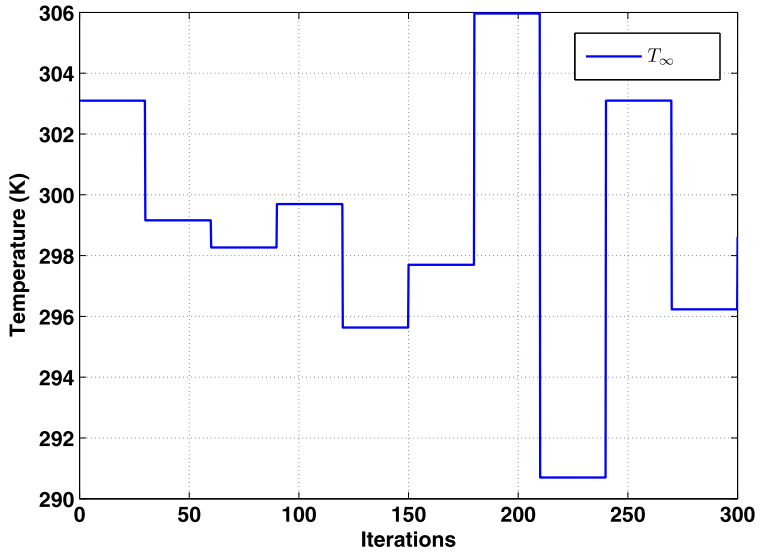

Fig. 9. The signal of disturbance: inlet temperature T_∞.

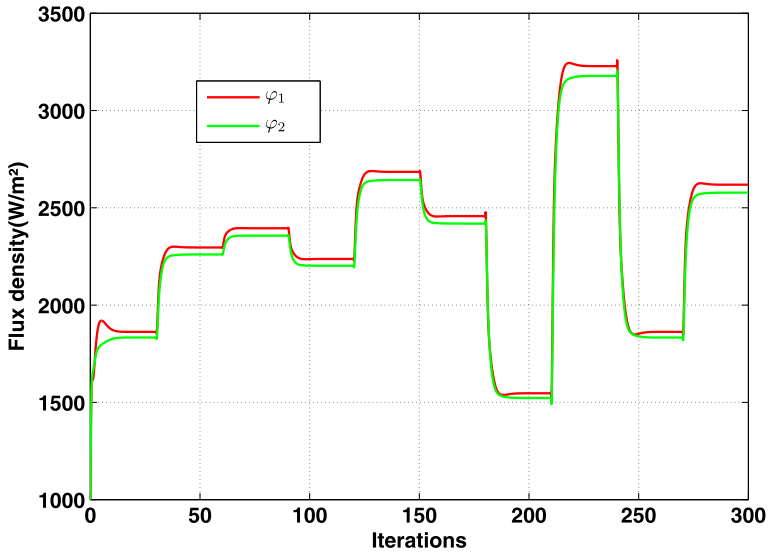

Fig. 10. The obtained command law $\boldsymbol{u} = [\varphi_1(t), \varphi_2(t)]^T$.

According to Table 1, it can be seen that the best minimization is obtained for the highest order. The increase of the order model from 6 to 10 does not decrease significantly the cost function. For our study, the order 6 gives satisfying enough results. This model is the one that shall be used for validation and used within control procedures.

The input fluxes used for validation are presented in Fig. 5. The resulting temperature evolutions in some outputs (location of the maximum error) for both the detailed model and the reduced model are presented in Fig. 6. One can see that the temperature evolutions and profiles computed with both the detailed and the reduced model are in very good agreement, the maximum temperature difference between both models being negligible when compared to orders of magnitude of the temperature steps.

Further, the obtained reduced model of order 6 will be the one used for solving optimal control problems, this model being assumed to approximate sufficiently well the physical behavior of the heated flow over the concerned backward-facing step. It is emphasized that the required CPU time for solving the full original flow problem along with the related energy problem was about a couple of hours. In the other hand, the CPU time required for running the reduced models was less than 0.1 s on the same computer.

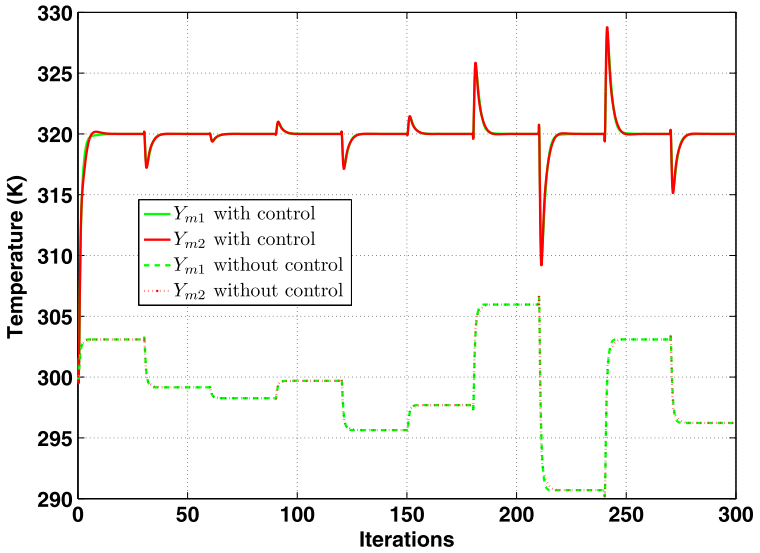

Fig. 11. The signal of the output temperature $\boldsymbol{y} = [Y_{m1}, Y_{m2}]^T$.

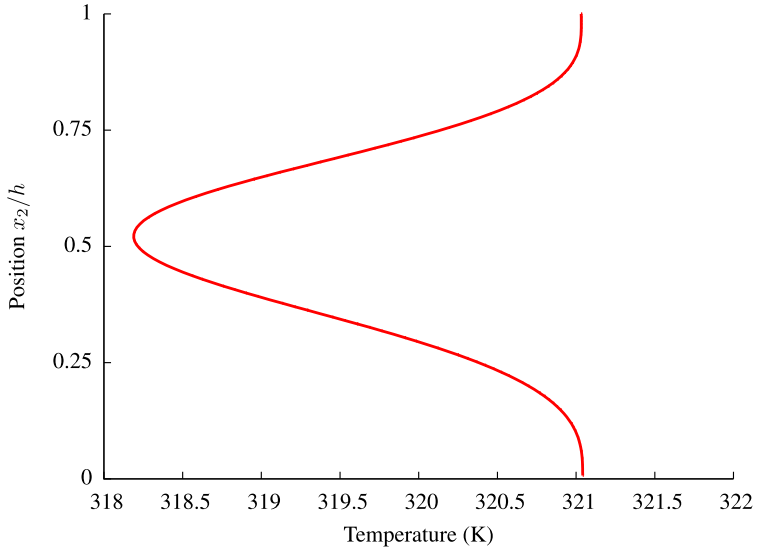

Fig. 12. Temperature profile obtained with $\bar{u}$ and $T_\infty = 300$ K.

5. Control application

The goal of this section is to show the feasibility and ability of the approach that combines the model reduction with the optimal control theory. There exists other applications combining these two approaches, among which one can quote [20–24]. As far as we are concerned, we propose to use a ROM identified by the MIM to determine a control law in order to control a temperature profile at the outflow of a pipe. We are interested in the reduced model of order $n = 6$ identified and developed in the previous section. Recall that this model is based on three inputs, and has an observable vector of dimension 135 located on the line $x_1/h = 16$. The flow is heated by both flux densities placed just upstream of the step and there is a temperature fluctuation around a nominal value (that must be counteracted) at the channel entrance (see Fig. 7). We propose in this study different control problems:

- the first control problem concerns the regulation problem (with a constant target), where the aim is to control two mean temperatures among 135 observables with the two input fluxes φ_1 and φ_2 by using the PID controllers;
- the second control problem is another regulation problem (still with a constant target), where the objective is to control all 135 observables by the two input fluxes φ_1 and φ_2; this control problem features the LQG algorithm;

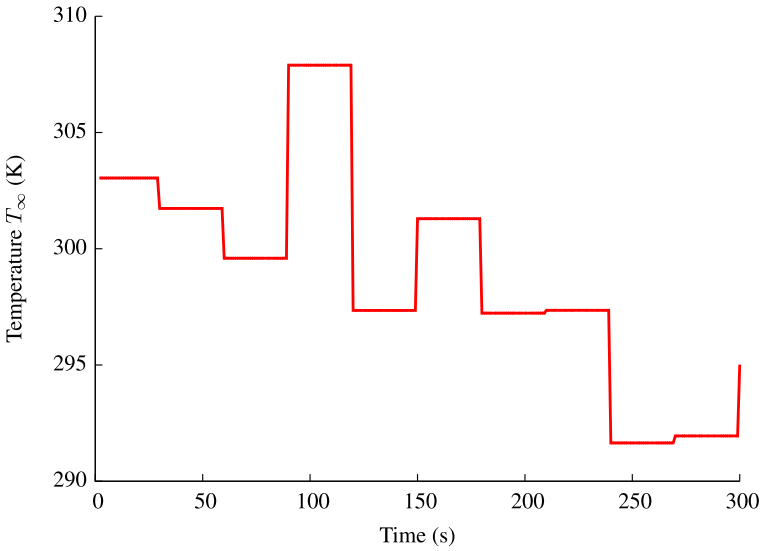

Fig. 13. Perturbation $T_\infty(t)$.

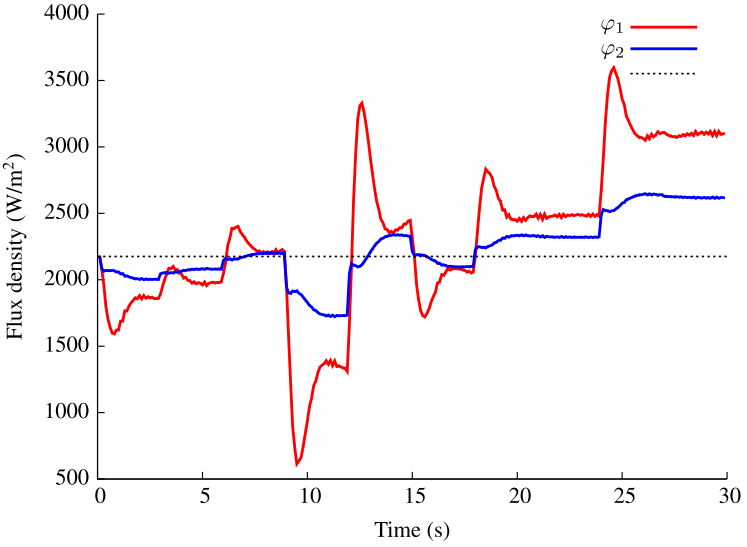

Fig. 14. Optimal command $u = [\varphi_1(t), \varphi_2(t)]^T$.

– the third control problem is a tracking problem (with a varying target) dealing again with the 135 observables placed on a virtual line close to the pipe outflow at $x_1 = 16h$.

5.1. Regulation problem: two inputs to control two outputs

In this first test problem, the output vector of the ROM is decomposed into two parts: the upper part Y_{m1} which contains the average of half of the observables values (from 1 to 68) and the bottom part Y_{m2} that contains the average of the remaining values of the observables (from 69 to 135).

One formulates the optimal control problem as: "whatever the supposed unknown disturbance of the inlet temperature T_∞, one seeks the optimal inputs $\boldsymbol{u} = [\varphi_1(t), \varphi_2(t)]^T$ so that the output vector $\boldsymbol{y} = [Y_{m1}, Y_{m2}]^T$ is as close as possible to a constant vector determined by the user (e.g. $\boldsymbol{y}_c = [320, 320]$ K)". In this control problem we have two inputs to control two outputs. The block diagram of the PID controller is given in Fig. 8. The signal of disturbance, that is the evolution of the inlet temperature is plotted in Fig. 9. The results of this control application in terms of the obtained command and the output thermograms are given in Figs. 10 and 11. One can note that the obtained control law acts in a significant way to counteract the disturbance and highly reduces the gap between the desired temperature and the output one.

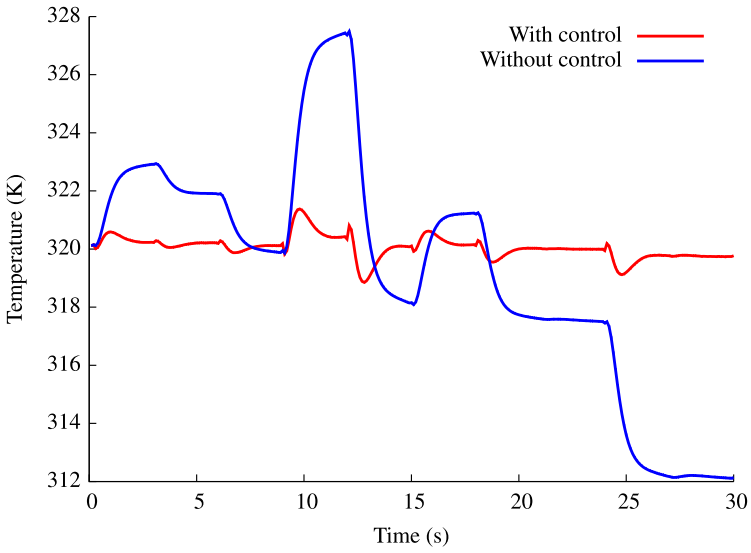

Fig. 15. Temperature evolution at $x_2 = \frac{3h}{2}$.

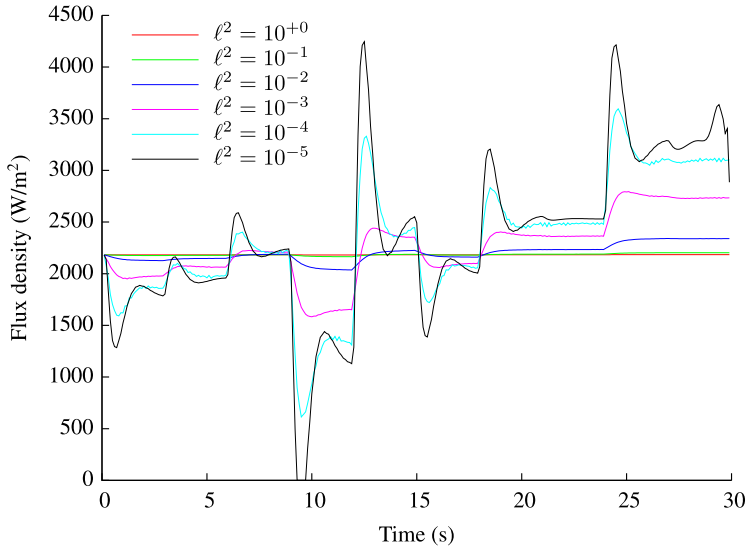

Fig. 16. Contribution of the ℓ_p^2 parameter on the evolution of the input φ_1.

5.2. Regulation problem: two inputs to control 135 outputs

In this section, our objective is to implement an algorithm which makes it possible to control the temperature profile (135 outputs) located on $x_1/h = 16$ by acting on the flux densities (2 inputs) situated upstream of the step. One formulates the optimal control problem: "whatever the supposed unknown disturbance of the inlet temperature $T_\infty(t)$, one seeks the optimal inputs $\boldsymbol{u} = [\varphi_1(t), \varphi_2(t)]^T$ so that the output vector $\boldsymbol{y} \in \mathbb{R}^{135}$ is as close as possible to a constant vector determined by the user (e.g. $\boldsymbol{y}_c = \mathbf{320} \in \mathbb{R}^{135}$ K)". In this control problem we have two inputs to control 135 outputs. When compared to the previous PID controller, the feedback control with a Linear Quadratic Regulator (LQR) allows to implement this kind of control problem. To do so, the control law is based on the deviation δx between the actual state x and the optimal steady-state $\bar{x}$ rather than on output y. In order to find $\bar{u}$ and $\bar{x}$ implicitly involved in (10), the following overdetermined system (with no perturbation) is solved:

$$\left(S^T S\right)\bar{u} = S^T y_c \tag{32}$$

where S is the sensitivity matrix $S = -ca^{-1}b$. Then $\bar{x}$ is obtained by $\bar{x} = -a^{-1}b\bar{u}$.

Fig. 12 presents the optimal temperature profile along $x_1 = 16h$ obtained with $\bar{u}$ and without perturbation (i.e. with $T_\infty = 300$ K). We note that without disturbance, the command $\bar{u}$ allows a close temperature profile to the set 320 K. However, in the presence of disturbances, i.e. when the temperature at the entrance of channel $T_\infty(t)$ varies, the command

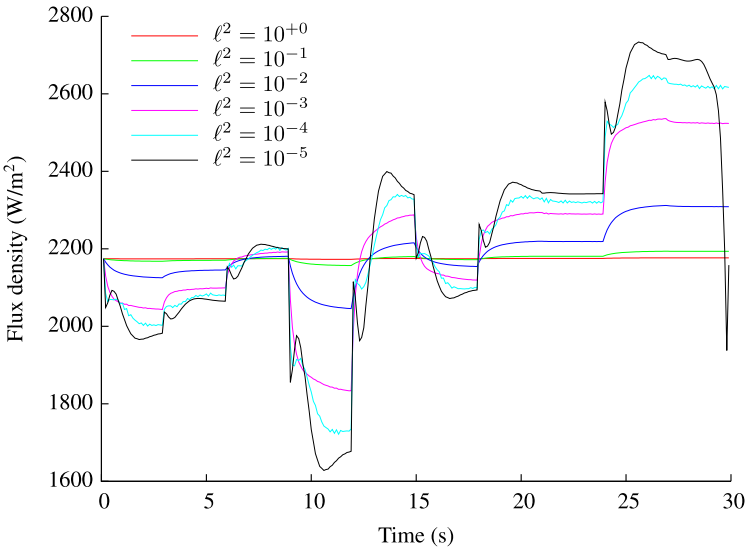

Fig. 17. Contribution of the ℓ_p^2 parameter on the evolution of the input φ_2.

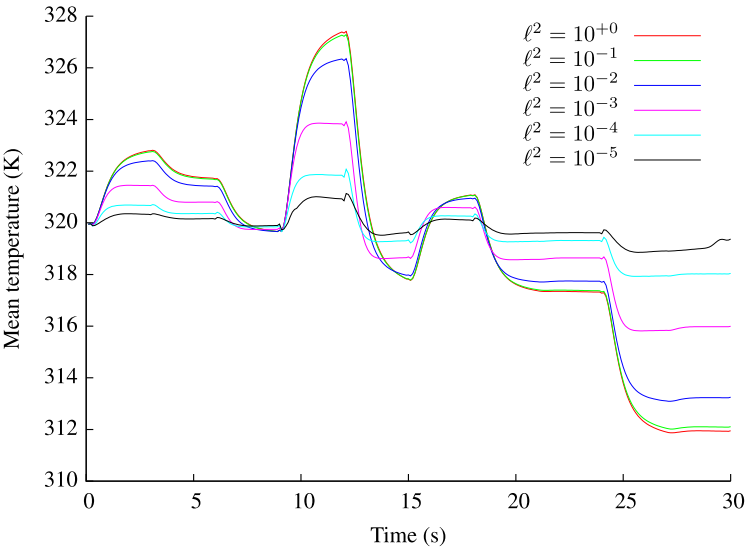

Fig. 18. Contribution of the ℓ_p^2 parameter on the evolution of the mean temperature.

$\bar{u}$ is no more valid. The objective is thus, when the inlet temperature T_∞ is disturbed with the signal of Fig. 13, to find the command allowing to correct this influence and to make the obtained temperature as close as possible to 320 K. The Kalman filter is used at this stage to estimate the state x of order 6 from 3 temperature measurements placed at $x_1 = 16h$ and for vertical positions $x_2 = \frac{h}{2}$, $x_2 = h$ and $x_2 = \frac{3h}{2}$ (see Fig. 7). The obtained optimal input $u = [\varphi_1(t), \varphi_2(t)]^T$ is reported in Fig. 14. The temperature evolution at $x_2 = \frac{3h}{2}$ is plotted in Fig. 15. We can note that the uncontrolled temperature is far away from 320 K. The obtained optimal law (Fig. 14) allows to reduce drastically this discrepancy.

These results are relative to a regulation problem with the parameter $\ell_p^2 = 10^{-4}$. We further analyze the sensitivity of the results to this parameter. Let us recall that in the criterion to be minimized, the parameter ℓ_p^2 comes to balance the effect of the command u: to have a weak δu it is necessary to give a raised value to ℓ_p^2; the goal of this parameter is to attenuate the use of excessive controls. One presents in Figs. 16 and 17 the evolutions of the optimal commands and in Fig. 18 the evolution of the corresponding space-mean output temperature, for different values of ℓ_p^2. As it was planned, the variations of u decrease as ℓ_p^2 increases (10^{-5} to 1). The value $\ell_p^2 = 1$ crushes the variation of the obtained command u. For a low value of ℓ_p^2 (for example $\ell_p^2 = 10^{-5}$) the optimal commands present strong fluctuations. In return, this value allows us to obtain the best results in terms of temperature outflow (cf. Fig. 18). According to all these curves, we thus see that the adjustment of the value of ℓ_p^2 corresponds to a compromise between acceptable fluctuations in inputs and deviations from the target.

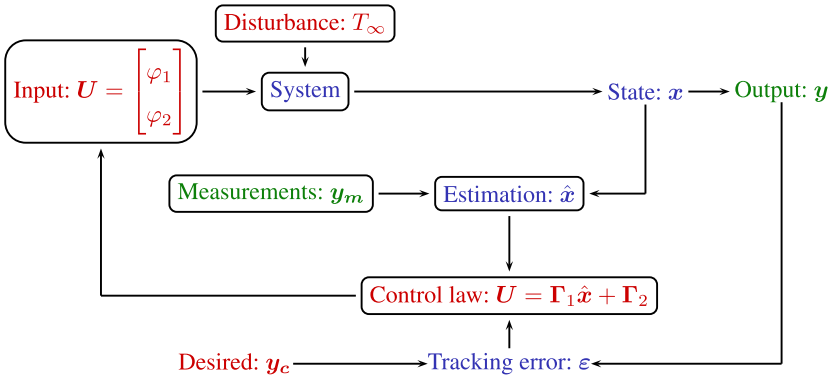

Fig. 19. Block diagram of the tracking problem with the state estimation.

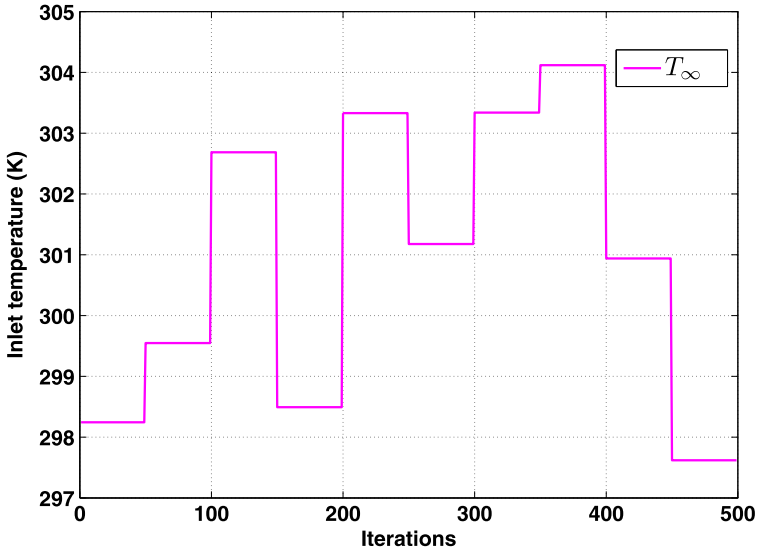

Fig. 20. The signal of disturbance: inlet temperature $T_\infty(t)$.

5.3. Tracking problem: two inputs to control 135 outputs

Previous sections concerned regulation problems where the desired output was constant. This section now gives an illustration of the tracking problem when the desired output is varying in time. The block diagram of this algorithm is given in Fig. 19, and the results of this application are presented in Figs. 20, 21 and 22.

The measurements $\boldsymbol{y}_m$ (of dimension 3 in this case) and Kalman filter model are used to estimate the state $\hat{\boldsymbol{x}}$ (of dimension 6) and deduce the control low $\boldsymbol{U} = (\varphi_1, \varphi_2)^t$ that counteracts the disturbance T_∞ from the computation of the gains $\boldsymbol{\Gamma}_1$ and $\boldsymbol{\Gamma}_2$.

In Fig. 20 we plot the signal of the disturbed inlet temperature $T_\infty(t)$. The obtained control law $\boldsymbol{u} = [\varphi_1(t), \varphi_2(t)]^T$ is plotted in Fig. 21. The temperature evolution at point (A) as well as the target temperature are given in Fig. 22. In this figure, we give also the evolution of the mean of the whole temperature profile. As it can be seen, the control law is acting efficiently to reduce the discrepancy between the evolutions of the output and of the desired temperature.

6. Conclusion

This study presented three feedback optimal control applications using a Reduced Order Model based on the Modal Identification Method and applied to a convection–diffusion problem. Two problems concerned regulation while the other one dealt with a tracking problem. A Kalman filter has been designed to evaluate the state from a few simulated points. If this system had been treated by a classic modeling, the corresponding model would not have allowed the control. That is the reason why a reduction technique has been used. The Modal Identification Method, which rests on an inverse problem of parameter estimation, is well suited for convection–diffusion processes. This study also showed that the Modal Identification Method seems to be efficient when being coupled with feedback controllers, integrating unknown perturbations and a filter

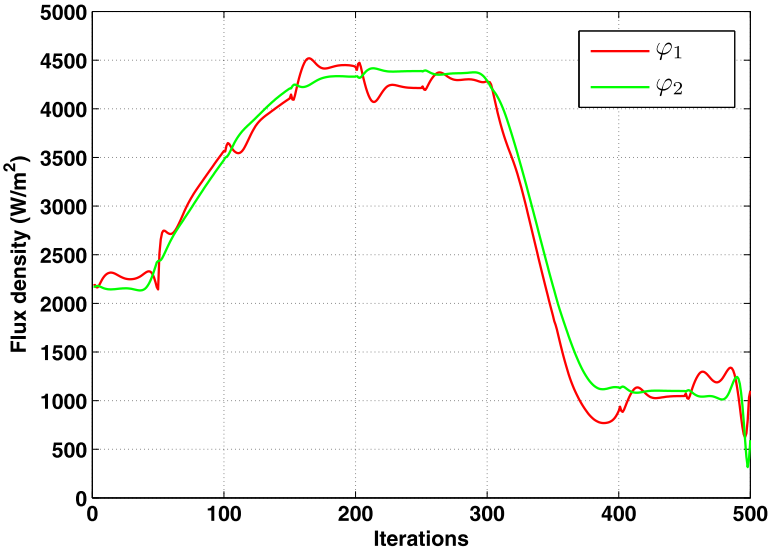

Fig. 21. The obtained command law $\boldsymbol{u} = [\varphi_1(t), \varphi_2(t)]^T$.

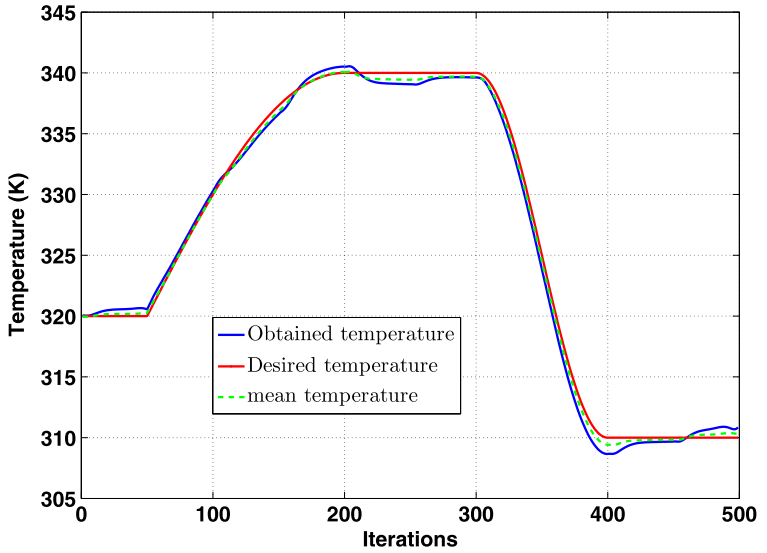

Fig. 22. Evolution of the target temperature, temperature at A point, and mean temperature.

to reconstruct the consequently unknown state. Next steps will include the coupling with some fluid mechanics reduced models in order to integrate some input velocity within the command.

References

[1] W.H.A. Schilders, H.A. Van der Vorst, J. Rommes, Model Order Reduction: Theory, Research Aspects and Applications, Mathematics in Industry, vol. 13, Springer, 2008.
[2] D.J. Lucia, P.S. Beran, W.A. Silva, Reduced-order modeling: new approaches for computational physics, Prog. Aerosp. Sci. 40 (1–2) (2004) 51–117.
[3] A.C. Antoulas, An overview of approximation methods for large-scale dynamical systems, Annu. Rev. Control 29 (2) (2005) 181–190.
[4] R. Pasquetti, D. Petit, Analyse modale d'un processus de diffusion thermique : identification par thermographie infrarouge, Int. J. Heat Mass Transf. 31 (3) (1988) 487–496.
[5] M. Girault, D. Petit, Identification methods in nonlinear heat conduction. Part I: Model reduction, Int. J. Heat Mass Transf. 48 (January 2005) 105–118.
[6] O. Balima, Y. Favennec, D. Petit, Model reduction for heat conduction with radiative boundary conditions using the modal identification method, Numer. Heat Transf., Part B 52 (2007) 107–130.
[7] O. Balima, Y. Rouizi, Y. Favennec, D. Petit, Reduced modelling through identification on 2D incompressible laminar flows, Inverse Probl. Sci. Eng. 17 (3) (2009) 303–319.
[8] Y. Rouizi, Y. Favennec, J. Ventura, D. Petit, Numerical model reduction of 2D steady incompressible laminar flows: Application on the flow over a backward-facing step, J. Comput. Phys. 228 (6) (2009) 2239–2255.

[9] Y. Favennec, M. Girault, D. Petit, The adjoint method coupled with the modal identification method for nonlinear model reduction, Inverse Probl. Sci. Eng. 14 (2006) 153–170.
[10] P. Borne, G. Dauphin-Tangy, J.P. Richard, F. Rottela, I. Zambettakis, Commande et Optimisation des Processus, Editions Technip, 1990.
[11] A.R. Ruuskanen, A. Seppänen, S. Duncan, E. Somersalo, J.P. Kaipio, Using process tomography as a sensor for optimal control, Appl. Numer. Math. 56 (2006) 37–54.
[12] Y. Favennec, Y. Rouizi, D. Petit, On the use of reduced models obtained through identification for feedback optimal control problems in a heat convection–diffusion problem, Comput. Methods Appl. Mech. Eng. 199 (17–20) (2010) 1193–1201.
[13] B.F. Armaly, F. Durst, J.C.F. Pereira, B. Schonung, Experimental and theoretical investigation of backward-facing step flow, J. Fluid Mech. 127 (1983) 473–496.
[14] Fluent, http://www.fluent.com/.
[15] E. Erturk, Numerical solutions of 2D steady incompressible flow over a backward-facing step, Part I: High Reynolds number solutions, Comput. Fluids 37 (6) (2008) 633–655.
[16] Y. Zang, R.L. Street, J.R. Koseff, A non-staggered grid, fractional step method for time-dependent incompressible Navier–Stokes equations in curvilinear coordinates, J. Comput. Phys. 114 (1994) 18–33.
[17] Y. Rouizi, M. Girault, Y. Favennec, D. Petit, Model reduction by the modal identification method in forced convection: Application to a heated flow over a backward-facing step, Int. J. Therm. Sci. 49 (2010) 1354–1368.
[18] O. Balima, Y. Favennec, M. Girault, D. Petit, Comparison between the modal identification method and the POD-Galerkin method for model reduction in nonlinear diffusive systems, Int. J. Numer. Methods Eng. 67 (2006) 895–915.
[19] M. Minoux, Mathematical Programming, Theory and Applications, Wiley, 1986.
[20] M. Li, P.D. Christofides, Optimal control of diffusion–convection–reaction processes using reduced-order models, in: Networked and Complex Systems S.I. – Control of Networked and Complex Process Systems, Comput. Chem. Eng. 32 (9) (2008) 2123–2135.
[21] J.D. Stigter, N. Scheerlinck, B. Nicolaï, J.F. Van Impe, Optimal heating strategies for a convection oven, J. Food Eng. 48 (4) (2001) 335–344.
[22] M. Bergmann, L. Cordier, Optimal control of the cylinder wake in the laminar regime by trust-region methods and pod reduced-order models, J. Comput. Phys. 227 (16) (2008) 7813–7840.
[23] E. Videcoq, M. Girault, A. Piteau, Thermal control via state feedback using a low order model built from experimental data by the modal identification method, Int. J. Heat Mass Transf. 55 (2012) 1679–1694.
[24] M. Girault, É. Videcoq, Temperature regulation and tracking in a MIMO system with a mobile heat source by LQG control with a low order model, Control Eng. Pract. 21 (2013) 333–349.